

1 This manuscript has been submitted for publication to
2 **Geophysical Research Letters**. Please note that the
3 manuscript is under review and subsequent versions of
4 this manuscript may have different content. If accepted,
5 the final version of the manuscript will be available via the
6 'Peer-reviewed Publication DOI' link on this webpage.
7 Please feel free to contact the corresponding author.

8

9 **Detection and forecasting of shallow landslides: lessons from a natural laboratory**
10
11 **R. Bainbridge¹, M. Lim², S. Dunning¹, M.G. Winter³, A. Diaz-Moreno¹, J. Martin², H.**
12 **Torun², B. Sparkes⁴, M. Khan², N. Jin²**

13 ¹ Department of Geography, Newcastle University, Newcastle, NE1 7RU, UK.

14 ² Faculty of Engineering and Environment, Northumbria University, Newcastle, NE1 8ST,
15 UK.

16 ³ Winter Associates, Kirknewton, Midlothian, EH27 8AF, UK.

17 ⁴ Bridgeway Consulting, Bridgeway House, Riverside Way, Nottingham NG2 1DP, UK.

18

19 Corresponding author: Rupert Bainbridge (rupert.bainbridge@newcastle.ac.uk)

20

21

22 **Detection and forecasting of shallow landslides: lessons from a natural laboratory**

23

24 **R. Bainbridge¹, M. Lim², S. Dunning¹, M.G. Winter³, A. Diaz-Moreno¹, J. Martin², H.**
25 **Torun², B. Sparkes⁴, M. Khan², N. Jin²**

26 ¹ Department of Geography, Newcastle University, Newcastle, NE1 7RU, UK.

27 ² Faculty of Engineering and Environment, Northumbria University, Newcastle, NE1 8ST,
28 UK.

29 ³ Winter Associates, Kirknewton, Midlothian, EH27 8AF, UK.

30 ⁴ Bridgeway Consulting, Bridgeway House, Riverside Way, Nottingham NG2 1DP, UK.

31

32 Corresponding author: Rupert Bainbridge (rupert.bainbridge@newcastle.ac.uk)

33

34 **Key Points:**

- 35 • Debris flow occurrence has been constrained by discernible thresholds in rainfall
36 antecedence, intensity-duration and abrupt increases.
- 37 • Early detection and development of evolving slope hazards is achieved through novel
38 time-lapse image vector tracking.
- 39 • Event occurrence and flow development can be automatically detected with low-cost
40 seismic monitoring and hodogram analysis.

41 **Abstract**

42 Shallow landslides are a significant hillslope erosion mechanism and limited
43 understanding of controls on initiation and development results in persistent risk on linear
44 infrastructure. We present an inventory of 63 landslides (2007-2019) from the west of Scotland
45 and show the patterns and development of debris flows, accounting for 58% of landslide source
46 volume. Using rainfall data, we show that landslides are often triggered during abrupt changes
47 in the rainfall trend. We derive empirical antecedent precipitation (>62mm) and intensity-
48 duration (>10 hours) thresholds over which debris flows occur. Analysis shows the thresholds
49 are more effective at raising landslide alert levels than the current management plan. We use
50 novel time-lapse vector tracking to detect slope instabilities, quantify deformation rates and
51 indicate imminent failure. Seismometers are used to detect a debris flow and locate the source
52 area. The suite of sensors provides vital information to support operational decision-making
53 for infrastructure with complex slope hazards.

54 **Plain Language Summary**

55 Landslide hazards present risks to road users and economic activity when associated
56 with roads. Differences in the materials making up hillslopes determine landslide susceptibility
57 and weather conditions can change the materials, altering the likelihood of landslide
58 occurrence; these interrelated factors limit our understanding of what triggers landslides on a
59 site-by-site basis. It is important to understand landslide triggers at high-risk sites so that they
60 can be monitored or mitigated against. We present a new landslide record for a hillside above
61 a strategic road in the west of Scotland. Using rainfall data, in combination with recorded
62 landslides, we determine what rainfall conditions, both leading up to and at the point of
63 triggering movement, generate debris flows at this site. A time-lapse camera allows landslide
64 occurrence to be timed accurately and, using computer software, we calculate changes on the
65 slope between camera images to detect and monitor the early stages of debris flows, providing
66 vital early warning. Finally, we use a seismometer (usually used for earthquake monitoring) to
67 detect when a debris flow has occurred and pinpoint its location on the slope. These tools can
68 be used to monitor landslide hazards at this site and other at-risk sites on road networks.

69 **1 Introduction**

70 Debris flows are extremely rapid (>5 m/s), saturated debris-rich landslides from
71 hillslopes (Hungr et al., 2014). Shallow landslides translate into debris flows given favorable
72 material and fluidization conditions (e.g. Zimmerman et al., 2020). Debris flow runout potential
73 and capacity to entrain water and sediment make them a significant global hazard, particularly

74 where linear infrastructure traverses affected slopes (Geertsema et al., 2009; Meyer et al.,
75 2015). They can be broadly grouped into channelized debris flows (CDFs) that are constrained
76 for their flow path and hillslope debris flows (HDFs) that occur on non-incised slopes (Chen
77 et al., 2009). CDFs and HDFs can transition into one another where HDFs meet gullies or CDFs
78 breach channels and flow over slope; hillslope-gully coupling controls the hazard potential
79 (Milne et al., 2009). CDFs often occur in torrent systems, such as the Illgraben, Switzerland
80 (Badoux et al., 2009) where the repeated flow path removes some of the spatial risk uncertainty.

81 Where debris flows source across large areas with uncertain runout, a combination of
82 active mitigation (physically controlling site aspects using engineering infrastructure) and
83 passive mitigation (reducing impacts via land-use planning, closures and warning systems)
84 methods can be used (Huebl and Fiebiger, 2005; Vagnon, 2020).

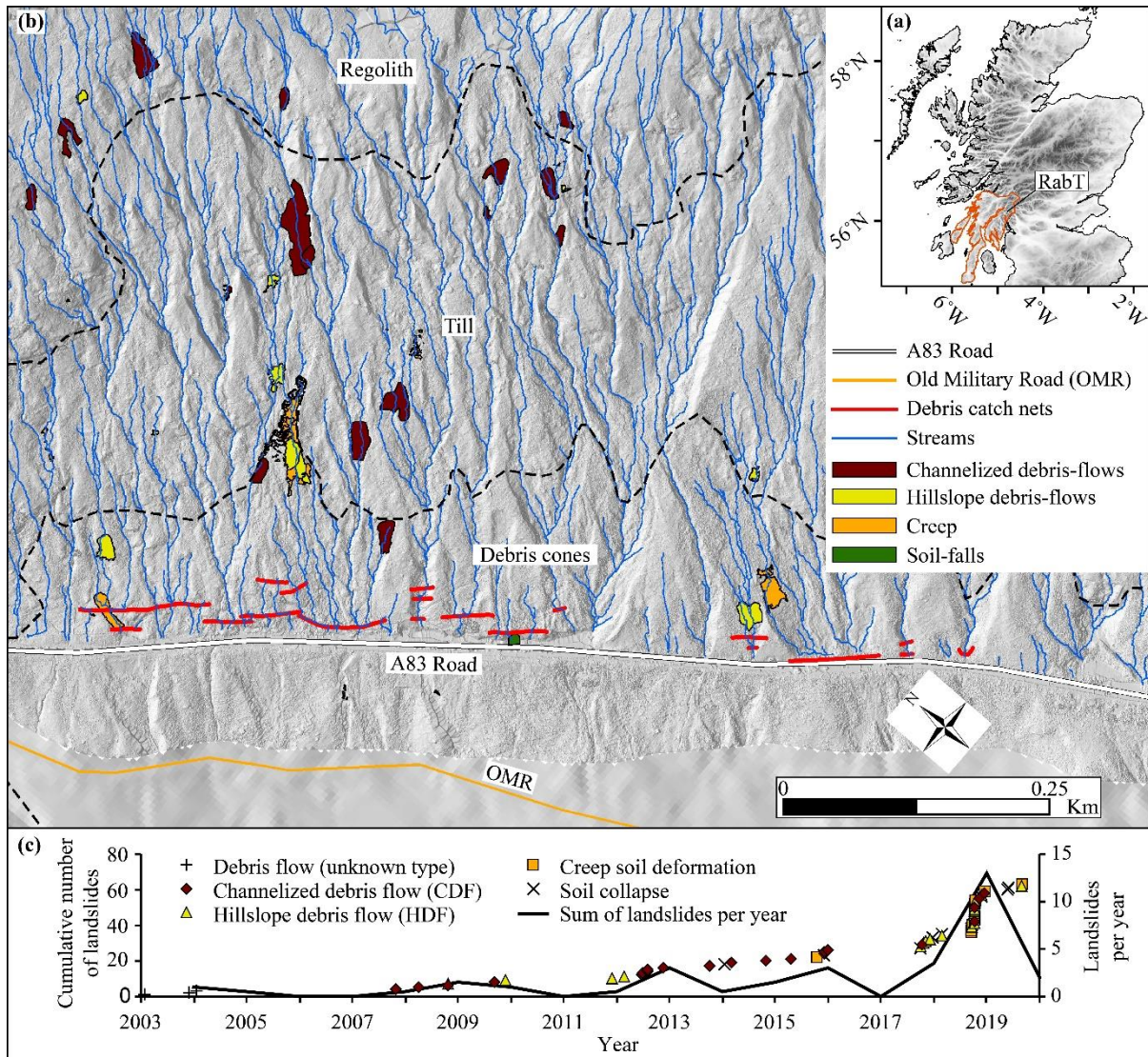
85 In Scotland, debris flows have repeatedly damaged linear infrastructure resulting in
86 economic and social costs (Winter et al. 2019a). Here we demonstrate a novel combination of
87 near-real-time, multi-disciplinary, monitoring techniques that allow remote detection and
88 quantification of slope changes and supplement Landslide Management Plans (LMP). The
89 objective of these techniques is to improve our understanding of shallow landslide trigger
90 mechanisms and creeping deformation that threaten road users and infrastructure, and thus
91 enhance alert capabilities for stakeholders at a debris flow prone site in the west of Scotland.

92 **2 Study area**

93 The A83 Rest and be Thankful (RabT), a key road into west Scotland, has the highest
94 landslide frequency on the Scottish road network (McMillan and Holt, 2019). It bisects the
95 south-western slope of Beinn Luibhean upslope from Glen Croe. The bedrock is Schist, with
96 overlying till up to 3 m thick, interspersed with gullies, scars, levees and debris cones (Sparkes
97 et al., 2017, Finlayson, 2020, BGS, 2020). Past debris flows have been linked to high-intensity
98 rainfall (Winter et al., 2019b).

99 On average 4,000 vehicles cross the RabT per day (Winter et al. 2019a). Closures divert
100 traffic ~88 km, if the Old Military Road (OMR), a one-way convoy diversion downslope of the
101 A83 is closed, casting a vulnerability shadow over 4,300 km² (Fig 1a). A full road closure
102 costs ~£90k per day (2012 prices; Winter et al. 2019a) and £13.3 M has been spent on
103 protecting the A83 and improving the OMR (Scottish Parliament, 2020). Some debris flows
104 still exceed mitigation measures and impact the A83 and OMR. Both semi-quantitative and
105 quantitative risk assessments (QRA) at the RabT justified measures for the LMP (Winter et al.,

106 2009; Winter and Wong, 2020) which sends out daylight patrols and activates warning lights
 107 on the RabT approach if forecast rainfall is ≥ 25 mm in a 24-hour period or ≥ 4 mm in a 3-
 108 hour period (Winter et al. 2020).



109

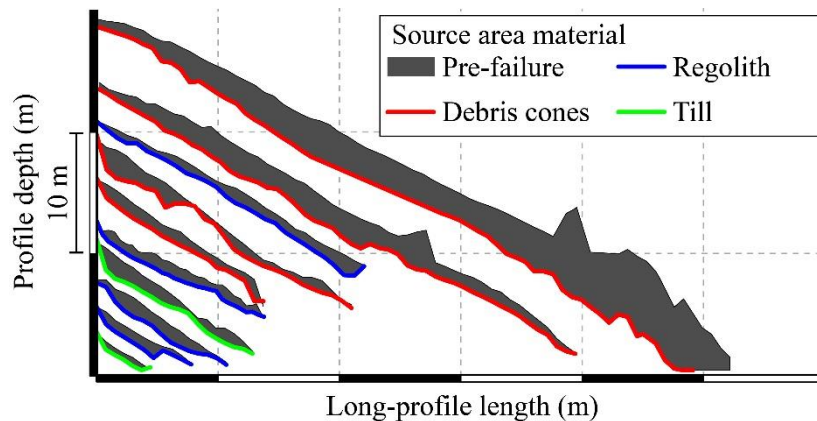
110 **Figure 1.** RabT landslide inventory. (a) Scotland digital terrain model showing the RabT site
 111 and area affected by an A83 road closure outlined in orange (vulnerability shadow, modified
 112 from Winter et al. 2019a). (b) TLS derived hillshade and 2007 to 2019 landslide source areas,
 113 colored by autumn-winter season (Sept-Feb), Spring (Spr) or Summer (Sum). Surface material
 114 delineation (dashed lines) modified from Finlayson, 2020. Landslide numbers refer to Fig 3.
 115 (c) 2003 to 2019 cumulative landslide timeseries and yearly totals.

116 3 Landslide activity

117 We have collated a new RabT landslide inventory from road reports (2003-2015),
 118 quarterly and event responsive terrestrial laser scans (TLS; 2015-2019) and time-lapse imagery
 119 (2017-2020). Post-2015 it is unlikely events are missing as TLS (0.1 m resolution) and time-
 120 lapse imagery was used (Sparkes et al., 2017 and this study). Pre-2015, debris flows that

121 reached the A83 are recorded, but smaller landslides may not be. From 2003 to 2019 there were
 122 63 landslides; 43 were debris flows (19 HDFs, 21 CDFs, three of unknown type), 11 slope
 123 creeps (slow gravitational deformation of material), and nine soil collapses (small $\sim 1\text{m}^3$ failures
 124 of surficial material, often from the top of bedrock outcrops, which do not propagate
 125 downslope). Fifteen debris flows closed the A83, on average nearly once a year since 2003; six
 126 reached the OMR.

127 60 landslides have known source areas (Fig. 1b), 45% (n=27) are in till, 35% (n=21) in
 128 debris cones and 20% (n=12) in regolith. 50 of these have source volumes derived from TLS
 129 (2015-2019) or estimates from reports (2007-2015). Debris cones cover 22% of the slope and
 130 account for 27% of the landslide volume; regolith (18% of the slope) and till (61% of the slope)
 131 account for 10% and 62% of the landslide volume respectively. Volumetric contributions from
 132 different materials reflect failure processes and depth to bedrock. Debris cone sources are
 133 generally long (15-30 m) and deep (average depth of 1.6m) and the slope of the failure plane
 134 is relatively shallow (average 31.5° ; Fig. 2). Till and regolith failure planes are steeper (average
 135 37° and 35° respectively) but generally short (5-15 m) with a shallower depth profile (average
 136 0.79 m and 0.77 m respectively; Fig. 2). Extrapolation of gully pathways in GIS, from a TLS
 137 derived DEM, shows a strong coupling of source areas and stream flow (streams in Fig. 1b).



138
 139 **Figure 2.** Landslide source area long profiles (2018-2019), derived from TLS point clouds,
 140 showing pre- and post-failure surface elevations. Profiles are colored by source material type.
 141 Axes are scaled together, one increment is 10m.

142 **4 Managing debris flow risk - Monitoring strategies for alert, tracking and detection**

143 Here we use 2018, an active year with 19 of the 63 landslides (Fig 1c), as a case study
 144 for pro-active, near-real-time monitoring to alert stakeholders to increased landslide risk based
 145 on rainfall thresholds, tracking slope creep, and detecting debris flow occurrence.

146 Rainfall on seasonal, daily, and 15-minute timescales has been used to indicate raised
147 landslide risk. The 2013-2019 seasonal rainfall trend was examined for Scottish Environment
148 Protection Agency (SEPA) RabT rain gauge data (SEPA, 2020) using the Bayesian Estimator
149 of Abrupt change, Seasonality and Trend (BEAST) analysis package (Zhao et al., 2019).
150 BEAST uses ensemble modelling, where multiple competing models analyze data, and
151 Bayesian statistics derive a model average with associated probabilities that detect if seasonal
152 and trend changes are ‘true’. BEAST identifies seasonal change points (SCPs) when rainfall
153 has large inter-annual variations, i.e. the seasonal component of the rainfall time-series changes
154 between the same time in different years. Trend change points (TCPs) are identified when the
155 rainfall time-series trend changes abruptly. For seasonal and trend components, not all
156 variations will lead to SCPs and TCPs being assigned, only those that have a high probability
157 of being a genuine and significant difference, based on the agreement between competing
158 models.

159 We calculated the Antecedent Precipitation Index (API; Fedora and Beschta, 1989), a
160 proxy for ground saturation (Segoni et al., 2018), for daily rainfall totals using Equation 1, as
161 an indicator of raised debris flow risk.

$$162 \quad API_i = k(API_{i-1}) + P_i \quad (1)$$

163 Where API_i is the API at time i , P_i is the daily rainfall total at i and k is a constant decay
164 function defined by the user ($k=0.8$). Rainfall was measured with an on-slope Davis Vantage
165 Pro 2 gauge, better reflecting on-slope conditions than the off-slope SEPA gauge.

166 Using 15-minute rainfall intensity data, we developed an intensity-duration (I-D)
167 threshold. Duration and mean rain intensity for all storms in the study period were plotted
168 (Brunetti et al., 2010; Guzzetti et al., 2008), with a six-hour inter-event period. An I-D threshold
169 above which landslides occur was visually derived from the results. Mean rain intensity over
170 an entire storm was used as not all landslide timings were known.

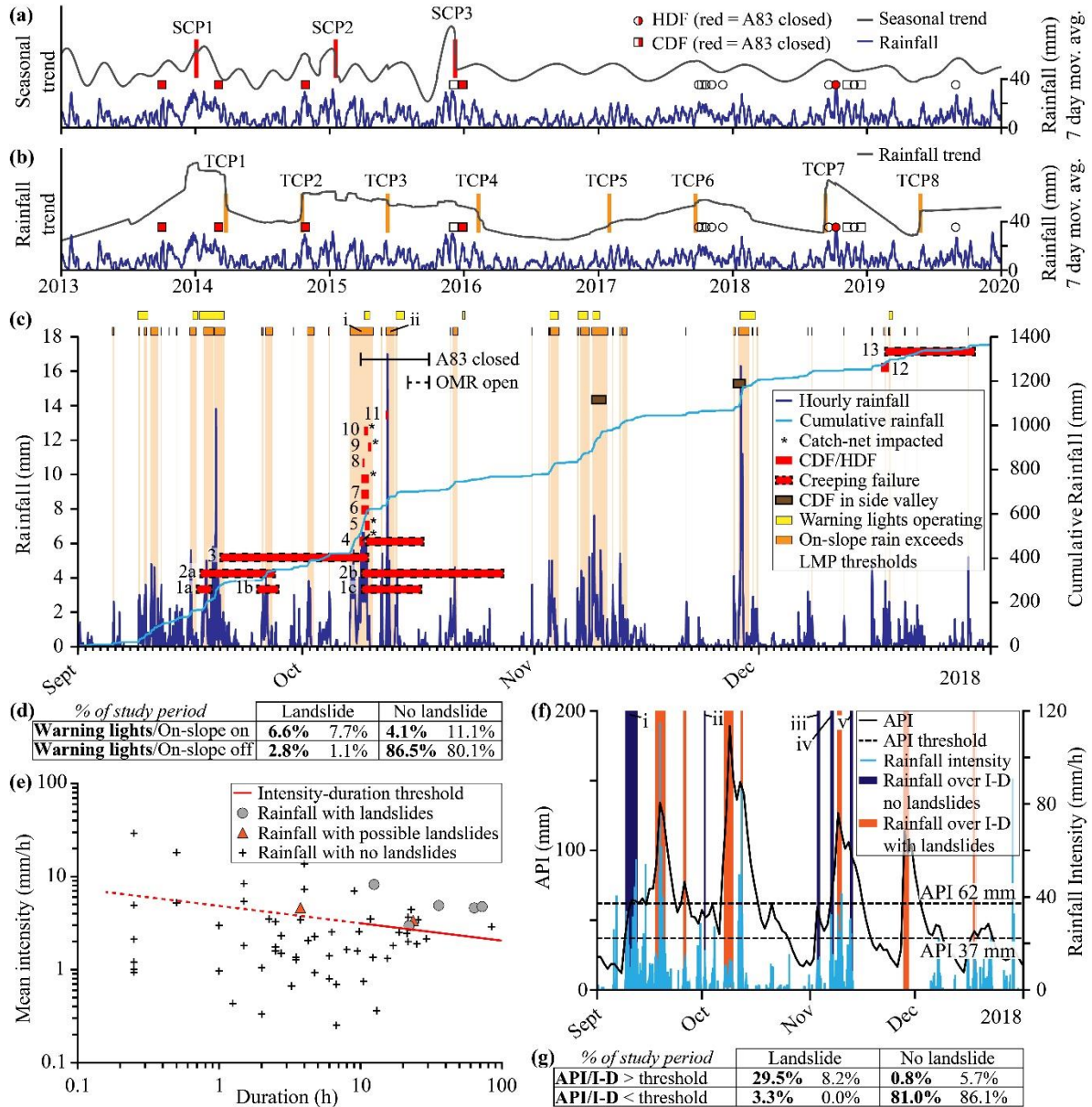
171 Alerts of slope changes allow stakeholders to be on stand-by, pre-position resources, or
172 proactively manage risk. Here, we process time-lapse imagery in a particle image velocimetry
173 tool (PIVLab; Thielicke and Stamhuis, 2014; Thielicke, 2020) to detect creep on the 19
174 September 2018. Displacement vectors and velocity were established between consecutive
175 slope-wide images at 16x16 pixel resolution ($\sim 2.7 \text{ m}^2$). Cumulative deformation was derived
176 for a point tracked through the photo sequence and inverse velocity (I-V), a tool used to predict
177 failure in brittle materials (Carlà et al., 2017), was used as a tentative metric for till failure

178 prediction despite the non-brittle materials involved. Imminent failure is predicted when I-V
179 values reach zero (infinite velocity). Intervals between images was not uniform due to poor
180 visibility, so velocity data from PIVLab were interpolated to 12h intervals, with a moving
181 average smoothing of 24h. I-V was calculated for smoothed data using $I/(Vw)$ (e.g. Manconi
182 and Giordan, 2016), where V is velocity over the defined time window (w).

183 We used seismic monitoring to detect debris flow onset. Seismometers are widely used
184 in torrent debris flows systems (Walter et al., 2017), but here a Raspberry Shake 3D
185 seismometer (Raspberry Shake, 2020; Manconi et al., 2018) was deployed for detection on a
186 hillslope with uncertain flow routing. The seismogram trace shows characteristic debris flow
187 signals, generated through clast-clast and flow-substrate interactions, above the long-term
188 average. Hodograms (plotting signal direction through time) were used to confirm the direction
189 of debris flow signals to the seismometer. Hodograms are seldom used in geosciences but have
190 been used in rockfall monitoring (Borella et al., 2019).

191 **5 Rainfall thresholds**

192 BEAST identified three rainfall seasonal change points (SCP) in winter periods from
193 2013 to 2016 (Fig. 3a). SCP3 coincides with Storms Desmond and Frank which caused debris
194 flows at the RabT. No SCPs are seen from 2016-2019. However, debris flows are coincident
195 with abrupt rainfall trend change points (TCPs) 2, 6 and 7, their subsequent falling trends and
196 in long period high trends (TCP1; Fig. 3b). TCP7 starts the 2018 landslide period. For this
197 period Fig. 3c shows when LMP forecast rainfall thresholds were exceeded and warning lights
198 were operating, along with the same thresholds plotted using on-slope, live rain data. These
199 data are summarized in confusion matrices (Fig. 3d and f) which describe the performance of
200 the rainfall thresholds in detecting conditions that triggered landslides; data are described as
201 times where thresholds predict landslides will or will not happen against times where landslides
202 did occur or not. False alarms and missed landslides account for 6.9% of the study period for
203 warning lights and 12.2% for on-slope data (Fig. 3d). Warning lights are human operated,
204 reducing false alarms through expert judgement. However, on-slope data would raise alert
205 levels two times where landslides occurred, that are not fully covered by the warning lights
206 (Fig. 3c i and ii). Landslide producing storms were medium (>10h) to long duration (max. 72h;
207 Fig. 3e); for two storms it is not known in which the landslide happened. Mean rain intensity
208 for landslide initiation ranges from 2.95 mm/hr to 8.15 mm/hr. Landslides occur above the
209 threshold described by Equation 2.



210

211 **Figure 3.** (a) BEAST seasonal rainfall component. (b) BEAST rainfall trend. (c) 01 September
 212 2018 to 31 December 2018 landslide timeline. (d) Warning light and on-slope alert operation
 213 confusion matrix. (e) September to December rainstorm intensity-duration (I-D) plot. (f)
 214 Antecedent Precipitation Index (API) with 37 mm and 62 mm thresholds. Rainfall intensity
 215 (data loss 13 November to 05 December) with storms >10h duration exceeding the I-D
 216 threshold. (g) API and I-D threshold confusion matrix.

217

$$I = 4.75D^{-0.18} \quad (2)$$

218

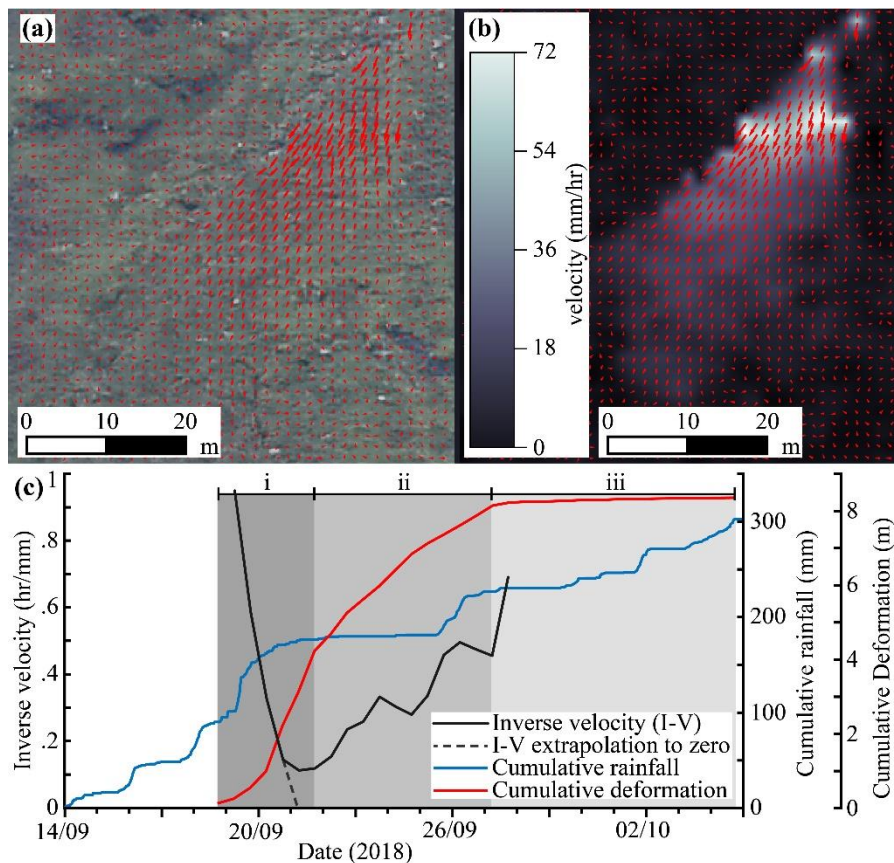
219 Where I is mean rain intensity and D is duration. As all confirmed landslide storms
 220 were >10h duration, the threshold may not apply to <10h storms. The I-D threshold gives a
 221 false alarm for 5.7% of the study period (Fig. 3g).

221

222 All landslides ($n=18$) occur over an API threshold of 37 mm, with three false alarms
 223 and long periods of alert with no landslides (Fig. 3f). A 62 mm API threshold covers 90% of
 224 landslides ($n=16$), reduces false alarms to 0.8% of the study period (Fig. 3g), but misses two
 225 mid-December events. A combination of I-D and API thresholds maximizes landslide detection
 226 and minimizes false alarms (Fig. 3g). All landslide inducing storms exceed the I-D threshold
 227 with five false alarms (Fig. 3f i to v) which API thresholds reduce to two (Fig. 3f iv, v).

228 6 Time-lapse vector tracking

229 We monitored the creep of Failure 2 (Fig. 3b) via time-lapse image vector tracking from
 230 initiation (19 September 2018) to arrest (27 September 2018) using PIVLab (Thielicke and
 231 Stamhuis, 2014; Thielicke, 2020; Khan et al., 2021). Vectors of change and a velocity heat map
 232 between consecutive images are shown in Figures 4a and 4b.



233

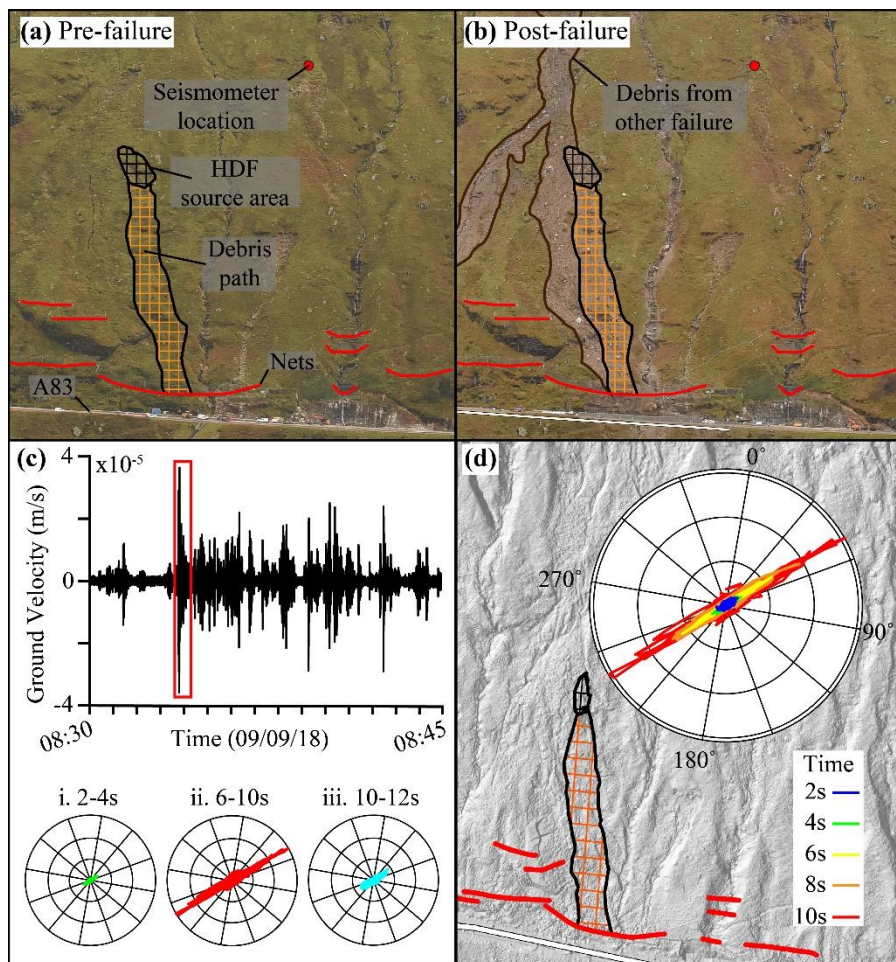
234 **Figure 4.** (a) PIVLab deformation vector plot (Thielicke and Stamhuis, 2014). (b) Velocity
 235 heat map. (c) Cumulative rainfall, cumulative deformation, and I-V.

236 Creep initiation coincides with a rainstorm on the 18 September 2018 (Fig. 4C i). Half
 237 of the total cumulative deformation occurs in the first 2.5 days. Inverse velocity (I-V) rapidly
 238 decreases towards zero on the 19-20 September 2018; extrapolation of the I-V trend predicts
 239 failure on the 21 September 2018. However, I-V values increase on the 21 September,

240 indicating reduced velocity after rainfall ceases. The deformation rate slows until arrest and
 241 subsequent rainfall does not affect the deformation rate (Fig. 4c ii and iii). Operationally, alert
 242 levels would be raised in Phase i when imminent failure seemed likely but lowered in Phase ii.

243 **7 Passive seismic debris flow detection**

244 Seismic monitoring identified a HDF (Figs. 5a and 5b) on the 09 October 2018 and
 245 located the source area. The z-axis seismogram (Fig. 5c) shows a high-amplitude signal lasting
 246 ~15s, corresponding with the failure time derived from time-lapse imagery, which is likely the
 247 HDF in motion. Short duration, lower amplitude signals follow and are likely post-landslide
 248 sediment and boulder reworking. Hodograms show very little activity at first (Fig. 5c i), but
 249 signal strength increases as the HDF signal arrives (ii) before subsiding (iii). Stacked
 250 hodograms, overlain on a DEM, point to the HDF source area as the direction of the incoming
 251 signal (Fig. 5d).



252
 253 **Figure 5.** (a) Pre-failure HDF source and seismometer location. (b) Post-failure. (c) Fifteen-
 254 minute seismogram with HDF signal (red box) and three hodogram time-steps (i, ii, iii). (d)
 255 Hillshade with HDF location and ten second stacked hodogram.

256 RabT debris flow seismic signals are brief due to short, steep flow paths, with boulder
257 and sediment reworking post-event. Another deposit on Fig. 5b, which is a thin, fine-grained
258 drape but has a large deposit footprint, was not detected by seismic monitoring; indicating that
259 whilst high debris content flows can be detected, hyper-concentrated flows may need larger
260 station arrays for detection.

261 **8 Discussion and conclusions**

262 This paper presents on-site monitoring at the RabT, aimed at supplementing the existing
263 LMP (Winter et al., 2009). Between 2003 and 2019 there are 63 landslides recorded, including
264 43 debris flows. Two landslide processes lead to debris flows, shallow translational slides
265 (mean depth c.1 m), generally below hydrological convergence zones in regolith and till, and
266 deep-seated (>2 m) rotational slides in debris cones. Material type exerts control on landslide
267 volumes. Total material export from source areas on the slope are 6,829 m³, with debris cones
268 accounting for 27% (1,853 m³), regolith 10% (697 m³) and till the remaining 63% (4,278 m³).

269 BEAST rainfall analysis shows that landslides are primarily associated with abrupt
270 rainfall trend changes. In the 2018 study period, antecedent, and medium- to long-duration,
271 high-intensity rainfall is shown to be an important factor in debris flows initiation. New local
272 API and I-D rainfall thresholds, identify all landslide inducing storms and minimize false
273 alarms, improve on the LMP and provide road authorities time to consider actions. 90% of
274 RabT landslides occurred over a 62 mm API, indicating a critical antecedent rainfall threshold.
275 Rainstorm I-D >10h is key for landslide initiation with largely higher mean rain intensity than
276 non-landslide storms. Shadow trials with confusion matrices against LMP thresholds are
277 needed before full deployment.

278 Time-lapse vector tracking located and quantified creeping deformation in response to
279 rainfall drivers. I-V calculations forecast imminent failure in the initiation phase, however
280 creep slowed when rainfall ceased and arrested despite further rainfall. This method can detect
281 slope movement and indicate times of heightened risk of failure for management authorities.

282 24-7 passive seismic detection and hodograms were used to identify a HDF. In this
283 instance, and likely others due to short RabT flow paths, the 15 second event duration is too
284 brief for live warnings but allows for 24/7 event detection and rapid response, outside of time-
285 lapse image capture. Additional seismometers (now deployed) extend the range of detection
286 and allow more traditional geo-location.

287 Our novel combination of sensors and processing techniques allows near-real-time
288 monitoring and quantification of shallow landslides as demonstrated at the RabT in the west of
289 Scotland. Results show that local sensor systems improve our understanding of triggers by
290 allowing landslides to be attributed to specific conditions due to better landslide timing
291 capabilities. This allows the forecasting of conditions that can likely induce landslides at this
292 site, however the techniques could be readily applied to other sites. Low-cost sensors can be
293 replicated at high- and lower-risk sites where cost-benefit would normally prevent monitoring.
294 Increased high-intensity rainfall due to climate warming is expected in Scotland (UKCP, 2018)
295 and more sites will have increased debris flow risk; greater low-cost monitoring capacity is a
296 necessary advancement.

297 **Acknowledgements**

298 We thank NERC (NE/P000010/1, NE/T00567X/1, NE/T005653/1), Research England
299 (www.Pitch-in.ac.uk ‘SlopeRIoT’), Transport Scotland and the Scottish Road Research Board
300 (SRRB) for funding. We also thank BEAR Scotland, GeoRope, Jacobs, Forestry and Land
301 Scotland, Glencroe Farm and John Mather for research, access, and on-site support. Datasets
302 for this research are available from the Newcastle University Data Repository
303 (<https://figshare.com/s/058074e7a14320a994ce>).

304 **References**

- 305 Badoux, A., Graf, C., Rhyner, J., Kuntner, R. and McArdell, B.W. (2009). A debris-flow
306 alarm system for the Alpine Illgraben catchment: design and performance. *Natural Hazards*,
307 *49*, 517-539, <https://doi.org/10.1007/s11069-008-9303-x>
- 308 BGS (2020). Onshore GeoIndex, <https://mapapps2.bgs.ac.uk/geoindex/home.html> (accessed
309 June 2020)
- 310 Borella, J., Quigley, M., Krauss, Z., Lincoln, K., Attanayake, J., Stamp, L. et al., (2019).
311 Geologic and geomorphic controls on rockfall hazard: how well do past rockfalls predict
312 future distributions? *Natural Hazards and Earth System Sciences*, *19*, 2249–2280,
313 <https://doi.org/10.5194/nhess-19-2249-2019>
- 314 Brunetti M.T., Peruccacci, S., Rossi, M., Luciani, S., Valigi, D. and Guzzetti, F. (2010).
315 Rainfall thresholds for the possible occurrence of landslides in Italy. *Natural Hazards and*
316 *Earth Systems Science*, *10*, 447-458. <https://doi.org/10.5194/nhess-10-447-2010>
- 317 Carlà, T., Intrieri, E., Di Traglia, F., Nolesini, T., Gigli, G and Casagli, N. (2017). Guidelines
318 on the use of inverse velocity method as a tool for setting alarm thresholds and forecasting
319 landslides and structure collapses. *Landslides*, *14*, 517-534. [https://doi.org/10.1007/s10346-](https://doi.org/10.1007/s10346-016-0731-5)
320 [016-0731-5](https://doi.org/10.1007/s10346-016-0731-5)
- 321 Chen, J-C., Lin, C-W., and Wang, L-C. (2009), Geomorphic Characteristics of Hillslope and
322 Channelized Debris Flows: A Case Study in the Shitou Area of Central Taiwan. *Journal of*
323 *Mountain Science*, *6*, 266-273. <https://doi.org/10.1007/s11629-009-0250-0>

- 324 Fedora, M.A. and Beschta, R.L. (1989). Storm runoff simulation using an Antecedent
325 Precipitation Index (API) model. *Journal of Hydrology*, *112*, 121-133.
326 [https://doi.org/10.1016/0022-1694\(89\)90184-4](https://doi.org/10.1016/0022-1694(89)90184-4)
- 327 Finlayson, A. (2020). Glacial conditioning and paraglacial sediment reworking in Glen Croe
328 (the Rest and be Thankful), western Scotland. *Proceedings of the Geologists' Association*,
329 *131(2)*, 138-154. <https://doi.org/10.1016/j.pgeola.2020.02.007>
- 330 Gertseema, M., Schwab, J.W., Blais-Stevens, A. and Sakals, M.E. (2009). Landslides
331 impacting linear infrastructure in west central British Columbia. *Natural Hazards*, *48*, 59-72.
332 <https://doi.org/10.1007/s11069-008-9248-0>
- 333 Guzzetti, F., Peruccacci, S., Rossi, M. and Stark, C.P. (2008). The rainfall intensity–duration
334 control of shallow landslides and debris flows: an update. *Landslides*, *5*, 3-17.
335 <https://doi.org/10.1007/s10346-007-0112-1>
- 336 Huebl, J. and Fiebigler, G. (2005). Debris-flow mitigation measures, in Jakob, M. and Hungr,
337 O., eds., *Debris-flow Hazards and Related Phenomena*, 445-487. Springer, Berlin Heidelberg
- 338 Hungr, O., Leroueil, S. and Picarelli, L. (2014). The Varnes classification of landslide types,
339 an update. *Landslides*, *11*, 167-194. <https://doi.org/10.1007/s10346-013-0436-y>
- 340 Khan, M.W., Dunning, S., Bainbridge, R., Martin, J., et al., (2021) Low-Cost Automatic
341 Slope Monitoring Using Vector Tracking Analyses on Live-Streamed Time-Lapse Imagery,
342 *Remote Sensing*, *13(5)*, 893, <https://doi.org/10.3390/rs13050893>
- 343 Manconi, A., Coviello, V., Galletti, M. and Seifert, R. (2018) Short Communication:
344 Monitoring rockfalls with the Raspberry Shake. *Earth Surface Dynamics*, *6*, 1219-1227.
345 <https://doi.org/10.5194/esurf-6-1219-2018>
- 346 Manconi, A. and Giordan, D. (2016). Landslide failure forecast in near-real-time. *Geomatics*,
347 *Natural Hazards and Risk*, *7:2*, 639-648. <https://doi.org/10.1080/19475705.2014.942388>
- 348 Meyer, N., Schwanghart, W., Korup, O. and Nadim, F. (2015). Roads at risk: traffic detours
349 from debris flows in southern Norway. *Natural Hazards and Earth System Science*, *15*, 985-
350 995. <https://doi.org/10.5194/nhess-15-985-2015>
- 351 McMillan, F.N. and Holt, C.A. (2018). BEAR Scotland NW trunk road maintenance:
352 efficient management of geotechnical emergencies. *Quarterly Journal of Engineering
353 Geology and Hydrogeology*, *52*, 286-294. <https://doi.org/10.1144/qjegh2018-035>
- 354 Milne, F.D., Werritty, A., Davies, M.C.R. and Brown, M.J. (2009). A recent debris flow
355 event and implications for hazard Management. *Quarterly Journal of Engineering Geology
356 and Hydrogeology*, *42*, 51–60. <https://doi.org/10.1144/1470-9236/07-073>
- 357 Raspberry Shake (2020). <https://raspberrysshake.org/> (accessed June 2020)
- 358 Segoni, S., Rosi, A., Lagomarsino, D., Fanti, R. and Casagli, N. (2018). Brief
359 communication: Using averaged soil moisture estimates to improve the performances of a
360 regional-scale landslide early warning system. *Natural Hazards and Earth System Science*,
361 *18*, 807-812. <https://doi.org/10.5194/nhess-18-807-2018>
- 362 SEPA, (2020). Rest and Be Thankful 15-minute rainfall record.
363 <https://www2.sepa.org.uk/rainfall/> (accessed May 2020)
- 364 Sparkes, B., Dunning, S., Lim, M. and Winter, M.G. (2017). Characterisation of Recent
365 Debris Flow Activity at the Rest and Be Thankful, Scotland, in Mikoš, M., Vilímek, V., Yin,
366 Y. and Sassa, K., eds., *Advancing Culture of Living with Landslides, Volume 5 Landslides in*

- 367 *Different Environments: WLF: Workshop on World Landslide Forum Conference*
368 *Proceedings*, 51-58. https://doi.org/10.1007/978-3-319-53483-1_8
- 369 Scottish Parliament (2020). Official Report of the Public Petitions Committee, 05 March
370 2020. <http://www.parliament.scot/parliamentarybusiness/report.aspx?r=12561> (accessed, July
371 2020)
- 372 Thielicke, W. (2020). PIVlab - particle image velocimetry (PIV) tool.
373 [https://www.mathworks.com/matlabcentral/fileexchange/27659-pivlab-particle-image-](https://www.mathworks.com/matlabcentral/fileexchange/27659-pivlab-particle-image-velocimetry-piv-tool)
374 [velocimetry-piv-tool](https://www.mathworks.com/matlabcentral/fileexchange/27659-pivlab-particle-image-velocimetry-piv-tool), MATLAB Central File Exchange. (Accessed July 2020)
- 375 Thielicke, W. and Stamhuis, E.J. (2014). PIVlab – Towards User-friendly, Affordable and
376 Accurate Digital Particle Image Velocimetry in MATLAB. *Journal of Open Research*
377 *Software*, 2 (1), e30. <http://doi.org/10.5334/jors.bl>
- 378 UKCP. (2018). UK Climate Projections. Met Office.
379 <https://www.metoffice.gov.uk/research/approach/collaboration/ukcp/> (accessed June 2020)
- 380 Vagnon, F. (2020). Design of active debris flow mitigation measures: a comprehensive
381 analysis of existing impact models. *Landslides*, 17, 313-333. [http://doi.org/10.1007/s10346-](http://doi.org/10.1007/s10346-019-01278-5)
382 [019-01278-5](http://doi.org/10.1007/s10346-019-01278-5)
- 383 Walter, F., Burtin, A., McArdell, B., Hovius, N., Weder, B., Turowski, J.M. (2017). Testing
384 seismic amplitude source location for fast debris-flow detection at Illgraben, Switzerland.
385 *Natural Hazards and Earth System Science*, 17, 939-955. [https://doi.org/10.5194/nhess-17-](https://doi.org/10.5194/nhess-17-939-2017)
386 [939-2017](https://doi.org/10.5194/nhess-17-939-2017)
- 387 Winter M.G., Macgregor F., Shackman, L. (2009). Scottish Road Network Landslides Study:
388 Implementation, The Scottish Executive, Edinburgh
- 389 Winter, M.G., Peeling, D., Palmer, D. and Peeling, J. (2019a). Economic impacts of
390 landslides and floods on a road network. *AUC Geographica*, 54 (2), 207-220,
391 <https://doi.org/10.14712/23361980.2019.18>
- 392 Winter, M.G., Ognissanto, F. and Martin, L.A. (2019b). Rainfall Thresholds for Landslides
393 Deterministic and Probabilistic Approaches. *Transport Research Laboratory Published*
394 *Project Report PPR901*, <https://trl.co.uk/reports/rainfall-thresholds-landslides>
- 395 Winter, M.G., Kinnear, N. and Helman, S. (2020). A technical and perceptual evaluation of a
396 novel landslide early warning system. *Proceedings, Institution of Civil Engineers*
397 *(Transport)*, <https://doi.org/10.1680/jtran.19.00138>
- 398 Winter, M.G. and Wong, J.C.F. (2020). The assessment of quantitative risk to road users
399 from debris flow. *Geoenvironmental Disasters*, 7(4), 1-19. [https://doi.org/10.1186/s40677-](https://doi.org/10.1186/s40677-019-0140-x)
400 [019-0140-x](https://doi.org/10.1186/s40677-019-0140-x)
- 401 Zhao, K., Wulder, M.A., Hu, T., Bright, R., Wu, Q., Qin, H., et al., (2019). Detecting change-
402 point, trend, and seasonality in satellite time series data to track abrupt changes and nonlinear
403 dynamics: A Bayesian ensemble algorithm. *Remote Sensing of Environment*, 232.
404 <https://doi.org/10.1016/j.rse.2019.04.034>
- 405 Zimmerman, F., McArdell, B.W., Rickli, C. and Scheidl, C. (2020). 2D Runout Modelling of
406 Hillslope Debris Flows, Based on Well-Documented Events in Switzerland. *Geosciences*,
407 *10(2):70*. <https://doi.org/10.3390/geosciences10020070>